11th International Conference on Engineering Vibration
Ljubljana, Slovenia, 7–10 September 2015

A NUMERICAL INVESTIGATION INTO THE EFFECT OF THE SUPPORTS ON THE VIBRATION OF ROTATING SHAFTS

A. A. Zakaria*[1], E. Rustighi[2], N. S. Ferguson[3]

Institute of Sound and Vibration Research, University of Southampton

[1]aaz1v13@soton.ac.uk

[2]er@isvr.soton.ac.uk

[3]nsf@isvr.soton.ac.uk

Keywords: Rotordynamics, Lateral Vibration, Bearings, Viscoelastic.

Abstract. *Vibration is typically encountered by rotating equipment during its start-up, running operation and shutdown. The severity of the oscillation, which depends on the critical speed and natural frequencies of the system, could cause serious malfunction of the device and affect its operating performance. A simplified lumped parameter model of a rotor system is typically used for the study of the shaft dynamics of a single rotor on bearing supports. Bearing supports are the means of connecting a device between the rotor and supporting structure, which are of different forms and designs. They can be a simple bushing, rolling-element or journal types for light, medium and large load applications respectively. Particularly in this work, flexible supports made of rubber are considered by implementing viscoelastic material into the rotor bearing system. Viscoelastic material is well known to be a good choice for use within isolation systems, due to it being easily available and possessing high damping characteristics over a wide temperature and frequency range. However, the change of mechanical properties with frequency and temperature makes it difficult to design a viscoelastically device that works over a large range of operating conditions. Thus numerical analysis, which focuses on the simple rotor model supported on a range of different flexible supports, will be presented and compared.*

1 INTRODUCTION

Rotating machinery is known to encounter lateral vibration during its range of operating service. Imbalance of uneven mass distribution of the rotor, instability of the supporting device or structure of the shaft and other potential external forces acting on the system can result in serious malfunction of the rotor-bearing system. As the operational speed varies, the critical speed and natural frequency of the system will alter accordingly and affect the performance of the system.

A simplified lumped parameter model of a rotor-bearing system is a popular model used to analyze the dynamics of single rotor supported on bearings. Bearings can be many forms, which depend upon specific assumptions, such as simple bushing, rolling-element and a wide range of journal types. These bearings are normally assumed to be attached on a fixed support, so that performance of the bearings can be evaluated specifically for the whole system dynamics.

In this work, the dynamics of a simple rotor-bearing system on flexible supports will be examined. As the system is supported on two bearings at the two ends of a shaft, it is assumed that the bearings will be mounted on flexible material. The main focus of this work is to implement viscoelastic material into the system. In parallel with the advancement of modelling viscoelastic material [1-7], which help to describe the complexity of the material properties, the application of viscoelastic components in rotordynamics has generally increased as well. Effects on the threshold speed, natural frequency and temperature sensitive behaviour on dynamics characteristics have been discussed in [8, 9] and [10] respectively as viscoleastic support properties vary. Furthermore viscoelastic supports in rotor-bearings systems are reported to be beneficial to attenuate noise and vibration [11, 12].

2 MATHEMATICAL MODEL

In this section, the mathematical modelling of a rigid rotor supported on flexible supports is demonstrated. Generally, the equations of motion of a rigid rotor mounted on flexible supports are derived where the latter are comprised of elastic or viscoelastic supports. The elastic support model is assumed to have a linear spring and viscous damping in parallel, while the viscoelastic support model is based on the standard linear model. For both type of supports, the rotor-bearing system is assumed to consist of a rigid rotor, a massless and rigid shaft supported on two identical short bearings, and the bearings are flexibly supported in both the horizontal and vertical directions.

A right-handed coordinate system is utilized to to define the motion of the rotor-bearing system as shown by Figure 1. The rigid rotor of mass m, spins around the Z-axis with angular velocity Ω and moves horizontally and vertically in the X and Y axes respectively. Gyroscopic couples act on the system by definition of angular momentum conservation that are perpendicular to the axis of spin. The direction of the moments about the X and Y axes are specified by angular direction of ψ and θ shown in Figure 1 respectively.

2.1 Viscously damped supports

From first principles, the equations of motion for the rigid rotor supported by viscously damped flexible supports including unbalance and external moments are

$$\begin{aligned} m\ddot{x} + c_{xT}\dot{x} + c_{xC}\dot{\psi} + k_{xT}x + k_{xC}\psi &= m\varepsilon\Omega^2\cos(\Omega t + \delta) \\ m\ddot{y} + c_{yT}\dot{y} - c_{yC}\dot{\theta} + k_{yT}y - k_{yC}\theta &= m\varepsilon\Omega^2\sin(\Omega t + \delta) \\ I_d\ddot{\psi} - I_p\Omega\dot{\theta} + c_{xC}\dot{x} + c_{xR}\dot{\psi} + k_{xC}x + k_{xR}\psi &= (I_d - I_p)\beta\Omega^2\cos(\Omega t + \gamma) \\ I_d\ddot{\theta} + I_p\Omega\dot{\psi} - c_{yC}\dot{y} + c_{yR}\dot{\theta} - k_{yC}y + k_{yR}\theta &= (I_p - I_d)\beta\Omega^2\sin(\Omega t + \gamma) \end{aligned} \tag{1}$$

where I_d and I_p are the diametral and polar moment of inertia of the rotor respectively. ϵ and β are the rotor eccentricity and skewed centerline angle respectively. δ and γ are the initial condition values of each horizontal, vertical and two angular displacements of the rotor.

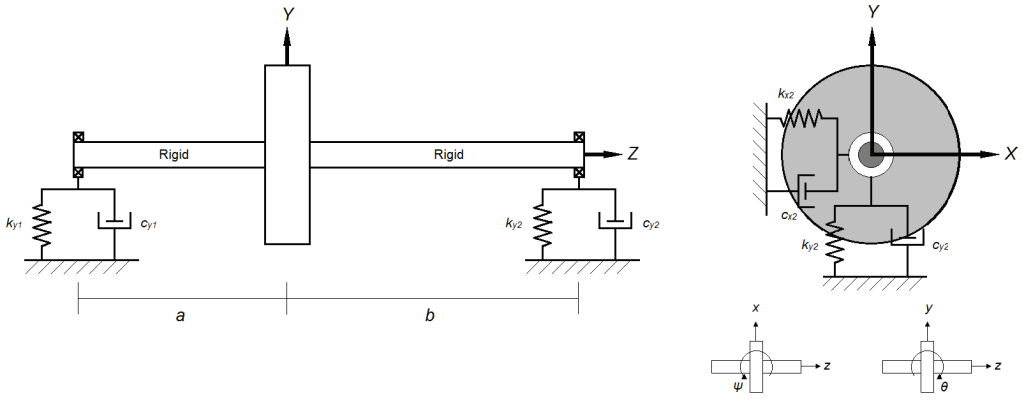

Figure 1: A rigid axisymmetric rotor on viscously damped supports and with definition of the coordinate system *X*, *Y*, and *Z*, origin at the static centre of mass of the rotor.

Stiffness and damping coefficients in Eq. (1) are expressed in term of a combination of each element from the two bearings by

$$\begin{aligned} S_{iT} &= S_{i1} + S_{i2} \\ S_{iC} &= -aS_{i1} + bS_{i2} \\ S_{iR} &= a^2S_{i1} + b^2S_{i2} \end{aligned} \tag{2}$$

where *S* are *k* or *c* for stiffness or damping coefficients respectively, and *i* is either *x* or *y*. The subscript *T*, *C* and *R* are used to describe the translational coefficient (*T*), coupling coefficient between translational and rotation (*C*) and rotational coefficient (*R*).

For free vibration analysis, all right hand terms in Eq. (1) are set to be 0. For convenience it can be converted to a state-space equation in the form of

$$\mathbf{A}\dot{\mathbf{x}} + \mathbf{B}\mathbf{x} = \mathbf{0} \tag{3}$$

where the arrangement of Eq. (1), as in Eq. (3) can be written as

$$\begin{bmatrix} \mathbf{C} & \mathbf{M} \\ \mathbf{M} & \mathbf{0} \end{bmatrix} \frac{\mathrm{d}}{\mathrm{d}t} \begin{Bmatrix} \mathbf{q} \\ \dot{\mathbf{q}} \end{Bmatrix} + \begin{bmatrix} \mathbf{K} & \mathbf{0} \\ \mathbf{0} & -\mathbf{M} \end{bmatrix} \begin{Bmatrix} \mathbf{q} \\ \dot{\mathbf{q}} \end{Bmatrix} = \begin{Bmatrix} \mathbf{0} \\ \mathbf{0} \end{Bmatrix} \tag{4}$$

where

$$\mathbf{A} = \begin{bmatrix} \mathbf{C} & \mathbf{M} \\ \mathbf{M} & \mathbf{0} \end{bmatrix}, \mathbf{B} = \begin{bmatrix} \mathbf{K} & \mathbf{0} \\ \mathbf{0} & -\mathbf{M} \end{bmatrix}, \dot{\mathbf{x}} = \frac{\mathrm{d}}{\mathrm{d}t} \begin{Bmatrix} \mathbf{q} \\ \dot{\mathbf{q}} \end{Bmatrix}, \mathbf{x} = \begin{Bmatrix} \mathbf{q} \\ \dot{\mathbf{q}} \end{Bmatrix} \tag{5}$$

The corresponding mass $\mathbf{M}$, damping and gyroscopic $\mathbf{C}$, and stiffness $\mathbf{K}$ matrices are

$$\mathbf{M} = \begin{bmatrix} m & 0 & 0 & 0 \\ 0 & m & 0 & 0 \\ 0 & 0 & I_d & 0 \\ 0 & 0 & 0 & I_d \end{bmatrix}, \mathbf{C} = \begin{bmatrix} c_{xT} & 0 & c_{xC} & 0 \\ 0 & c_{yT} & 0 & -c_{yC} \\ c_{xC} & 0 & c_{xR} & -I_p\Omega \\ 0 & -c_{yC} & I_p\Omega & c_{yR} \end{bmatrix}, \mathbf{K} = \begin{bmatrix} k_{xT} & 0 & k_{xC} & 0 \\ 0 & k_{yT} & 0 & -k_{yC} \\ k_{xC} & 0 & k_{xR} & 0 \\ 0 & -k_{yC} & 0 & k_{yR} \end{bmatrix} \tag{6}$$

and the degrees of freedom are represented as

$$\mathbf{q} = \begin{Bmatrix} x & y & \psi & \theta \end{Bmatrix}^T \tag{7}$$

The state-space matrix of Eq. (4) can be solved numerically for a single value rotor speed Ω and the respective complex eigenvalues S_n will represent the damping ratio ζ and damped natural frequency ω_d, which are in the form

$$\begin{aligned} s_n &= -\zeta_n + i\omega_{dn} \\ s_{n+4} &= -\zeta_n - i\omega_{dn} \end{aligned} \tag{8}$$

where n is 1,2, 3, or 4. The relationship between the damped natural frequency ω_{dn} and natural frequency of the particular system ω_n is assumed to be given, as for the single degree of freedom viscously damped system [13], by

$$\omega_{dn} = \omega_n \sqrt{1 - \zeta_n^2} \tag{9}$$

Since the motion of the rotor is defined in four degrees of freedom, so the roots of s_n and s_{n+4} form a complex conjugate pair for each n.

2.2 Viscoelastic supports

For viscoelastic materials, the viscously damped flexible supports in Figure 1 are replaced by the standard linear model viscoelastic supports that comprise an internal variable approach to incorporate the frequency dependence of the support modulus, as depicted in Figure 2

Referring to Figure 2, k_∞ is the stiffness constant, α and τ are viscoelastic material properties that can be obtained from material testing procedure [14]. Curve fitting of the data provides the τ and α coefficients which are used to determine the complex moduli behaviour of the viscoelastic component. From Figure 2, forces exerted on the bearings by viscoelastic supports are derived from first principle, which consider a single internal variable or degree of freedom *p*, at each support for both the *x* and *y* directions.

$$\begin{aligned} f_{x1} &= k_\infty(1+\alpha)(x - a\psi) - k_\infty \alpha p_{x1} \\ f_{y1} &= k_\infty(1+\alpha)(y + a\theta) - k_\infty \alpha p_{y1} \\ f_{x2} &= k_\infty(1+\alpha)(x + b\psi) - k_\infty \alpha p_{x2} \\ f_{y2} &= k_\infty(1+\alpha)(y - b\theta) - k_\infty \alpha p_{y2} \end{aligned} \tag{10}$$

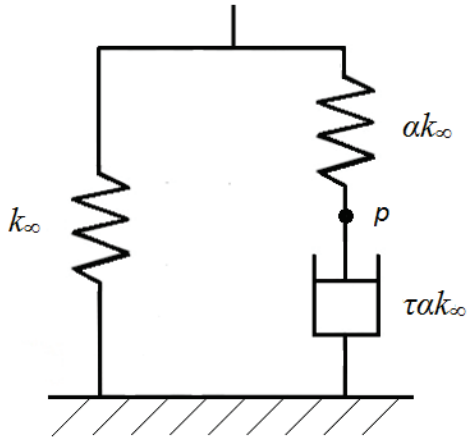

Figure 2: Standard linear model viscoelastic supports

By substituting Eq. (10) into Eq. (1), the equations of motion for rigid rotor mounted on identical viscoelastic supports are expressed as

$$\begin{aligned}
\ddot{x} &= -\frac{2\hat{k}}{m}x + \frac{\hat{k}(a-b)}{m}\psi + \frac{\hat{a}}{m}(p_{x1}+p_{x2}) + \varepsilon\Omega^2\cos(\Omega t+\delta)\\
\ddot{y} &= -\frac{2\hat{k}}{m}y - \frac{\hat{k}(a-b)}{m}\theta + \frac{\hat{a}}{m}(p_{y1}+p_{y2}) + \varepsilon\Omega^2\sin(\Omega t+\delta)\\
\ddot{\psi} &= \frac{I_p\Omega}{I_d}\dot{\theta} + \frac{\hat{k}(a-b)}{I_d}x - \frac{\hat{k}(a^2+b^2)}{I_d}\psi - \frac{\hat{a}a}{I_d}p_{x1} + \frac{\hat{a}b}{I_d}p_{x2} + \left(1-\frac{I_p}{I_d}\right)\beta\Omega^2\cos(\Omega t+\gamma)\\
\ddot{\theta} &= -\frac{I_p\Omega}{I_d}\dot{\psi} - \frac{\hat{k}(a-b)}{I_d}y - \frac{\hat{k}(a^2+b^2)}{I_d}\theta + \frac{\hat{a}a}{I_d}p_{y1} - \frac{\hat{a}b}{I_d}p_{y2} - \left(1-\frac{I_p}{I_d}\right)\beta\Omega^2\sin(\Omega t+\gamma)
\end{aligned} \tag{11}$$

where $\hat{k} = k_\infty(1+\alpha)$ and $\hat{a} = k_\infty\alpha$. By introducing the additional degrees of freedom, the equations of motion that describe the velocity displacement relationship of the internal variables can be written as

$$\begin{aligned}
\dot{p}_{x1} &= \frac{1}{\tau}(x - a\psi - p_{x1})\\
\dot{p}_{y1} &= \frac{1}{\tau}(y + a\theta - p_{y1})\\
\dot{p}_{x2} &= \frac{1}{\tau}(x + b\psi - p_{x2})\\
\dot{p}_{y2} &= \frac{1}{\tau}(y - b\theta - p_{y2})
\end{aligned} \tag{12}$$

The resulting equations of motion in Eqs. (11) and (12) can be written in state space equation [13] as

$$\dot{\mathbf{r}} = \mathbf{D}\mathbf{r} + \mathbf{w}(t) \tag{13}$$

where

$$\mathbf{r} = \begin{Bmatrix} \dot{\mathbf{q}} \\ \mathbf{q} \\ \mathbf{u} \end{Bmatrix} \tag{14}$$

as

$$\mathbf{u} = \begin{Bmatrix} p_{x1} & p_{y1} & p_{x2} & p_{y2} \end{Bmatrix}^T \tag{15}$$

and

$$\mathbf{D} = \begin{bmatrix} \bar{\mathbf{G}} & \bar{\mathbf{K}} & \bar{\mathbf{V}} \\ \boldsymbol{I} & \mathbf{0} & \mathbf{0} \\ \mathbf{0} & \bar{\mathbf{T}} & \bar{\mathbf{H}} \end{bmatrix} \tag{16}$$

Each element of $\mathbf{D}$ is 4×4 matrix where

$$\bar{\mathbf{G}} = \begin{bmatrix} 0 & 0 & 0 & 0 \\ 0 & 0 & 0 & 0 \\ 0 & 0 & 0 & \frac{I_p\Omega}{I_d} \\ 0 & 0 & -\frac{I_p\Omega}{I_d} & 0 \end{bmatrix}, \bar{\mathbf{K}} = \begin{bmatrix} -\frac{2\hat{k}}{m} & 0 & \frac{\hat{k}(a-b)}{m} & 0 \\ 0 & -\frac{2\hat{k}}{m} & 0 & -\frac{\hat{k}(a-b)}{m} \\ \frac{\hat{k}(a-b)}{I_d} & 0 & -\frac{\hat{k}(a^2+b^2)}{I_d} & 0 \\ 0 & -\frac{\hat{k}(a-b)}{I_d} & 0 & -\frac{\hat{k}(a^2+b^2)}{I_d} \end{bmatrix},$$

$$\bar{\mathbf{V}} = \begin{bmatrix} \frac{\hat{a}}{m} & 0 & \frac{\hat{a}}{m} & 0 \\ 0 & \frac{\hat{a}}{m} & 0 & \frac{\hat{a}}{m} \\ -\frac{\hat{a}a}{I_d} & 0 & \frac{\hat{a}b}{I_d} & 0 \\ 0 & \frac{\hat{a}a}{I_d} & 0 & -\frac{\hat{a}b}{I_d} \end{bmatrix}, \bar{\mathbf{T}} = \begin{bmatrix} \frac{1}{\tau} & 0 & -\frac{a}{\tau} & 0 \\ 0 & \frac{1}{\tau} & 0 & \frac{a}{\tau} \\ \frac{1}{\tau} & 0 & \frac{b}{\tau} & 0 \\ 0 & \frac{1}{\tau} & 0 & -\frac{b}{\tau} \end{bmatrix},$$

$$\bar{\mathbf{H}} = \begin{bmatrix} -\frac{1}{\tau} & 0 & 0 & 0 \\ 0 & -\frac{1}{\tau} & 0 & 0 \\ 0 & 0 & -\frac{1}{\tau} & 0 \\ 0 & 0 & 0 & -\frac{1}{\tau} \end{bmatrix}$$

For the forced vibration case, due to mass unbalance,

$$\mathbf{w}(t) = \begin{bmatrix} \varepsilon\Omega^2 \cos(\Omega t + \delta) \\ \varepsilon\Omega^2 \sin(\Omega t + \delta) \\ +\left(1 - \frac{I_p}{I_d}\right)\beta\Omega^2 \cos(\Omega t + \gamma) \\ -\left(1 - \frac{I_p}{I_d}\right)\beta\Omega^2 \sin(\Omega t + \gamma) \end{bmatrix}$$

$\mathbf{w}(t)$ can be set to zero for the free vibration case and then a standard eigenvalue problem has to be solved. Because of the additional degrees of freedom introduced from the internal variables as in Eq. (14), the complex conjugate eigenvalues of S_n of Eq. (8) are now expanded to six pairs instead of four.

3 NUMERICAL SIMULATIONS

In this section, several examples will be shown for the free vibration of a rigid rotor mounted on elastic, viscously damped and viscoelastic supports. Subsequently the forced vibration analysis will be presented for specifically a rotor-bearing system supported on identical viscoelastic supports at both ends. In general, the state space matrix solutions of $\dot{\mathbf{x}}$ and $\dot{\mathbf{r}}$ depend on the rotor rotational speed for Eqs. (3) and (14) respectively. It is convenient to determine the way in which the roots change with the rotational speed graphically by plotting a Campbell diagram where the rotational speed on a horizontal axis and the natural frequencies on vertical axis. Consider a uniform rigid rotor of mass $m = 122.68$ kg, diametral moment of inertia $I_d = 2.8625$ kgm^2 and polar moment of inertia $I_p = 0.6134$ kgm^2 mounted on flexible supports. The rotor is located at the geometric centre of the system, 0.25 m from each support.

3.1 Free vibrations

The parameter values for each support configuration are given in Table 1 specifically for free vibration analysis.

Type of Flexible Support	**Uncoupled system**	**Coupled system**
Undamped	$k_{x1} = 1.0$ MN/m	$k_{x1} = 1.0$ MN/m
	$k_{y1} = 1.5$ MN/m	$k_{y1} = 1.5$ MN/m
	$k_{x2} = 1.0$ MN/m	$k_{x2} = 1.3$ MN/m
	$k_{y2} = 1.5$ MN/m	$k_{y2} = 2.0$ MN/m
Viscously damped	$k_{x1} = k_{y1} = 1.0$ MN/m	$k_{x1} = k_{y1} = 1.0$ MN/m
	$k_{x2} = k_{y2} = 1.0$ MN/m	$k_{x2} = k_{y2} = 1.3$ MN/m
	$c_{x1} = c_{x2} = 1.0$ kNs/m	$c_{x1} = c_{x2} = 0.1$ kNs/m
	$c_{y1} = c_{y2} = 1.2$ kNs/m	$c_{y1} = c_{y2} = 0.3$ kNs/m
Viscoelastic	$k_\infty = 1.5$ MN/m	$k_\infty = 1.5$ MN/m
	$\alpha = 10$	$\alpha = 1$
	$\tau = 8.6667\text{x}10^{-4}$	$\tau = 8.6667\text{x}10^{-3}$

Table 1: Type of rigid rotor supports and its corresponding parameters for free vibration analysis. The uncoupled system corresponds to symmetric geometry of the rotor and shaft with equal supports at both ends

An example of a rigid rotor mounted on uncoupled anisotropic bearings produces the natural frequency map shown in Figure 3a. By substituting the corresponding parameters into Eq. (2), the coupling stiffnesses k_{xC} and k_{yC} are found to be zero. Thus, the first and second equations of Eq. (1), for which all the right hand terms are neglected, are uncoupled from the main system and are independent of rotor angular speed, Ω. Since the stiffnesses in both the horizontal and vertical directions are different, then the two natural frequencies that are determined from these equations in x and y are different. When the rotor is not rotating, the remaining two solutions of Eq. (1) are also uncoupled with two distinct natural frequencies. However as the rotor speed increases the two equations are coupled by gyroscopic terms and one of the natural frequency is decreasing whilst the other is increasing. It can be seen that the natural frequencies are converging on account of the gyroscopic effect. The decreasing line is one whereby the whirl is opposed to the rotor rotation direction, Ω and the increasing line is one where the whirl and the rotation directions, Ω are the same. The decreasing natural frequency also intersects with two constant natural frequencies lines at about 8000 and 13000 rev/min. This is a result of the equations of motion being uncoupled and independent of one another (i.e. x and ψ are

uncoupled as the terms in the equations satisfy $k_{xC}x = k_{xC}\psi = 0$).

The natural frequency map for a rigid rotor supported on coupled anisotropic bearings is depicted in Figure 3b. It can be seen from this figure that all of the natural frequency lines do not intersect, which imply all of the equations in Eq. (1) are coupled.

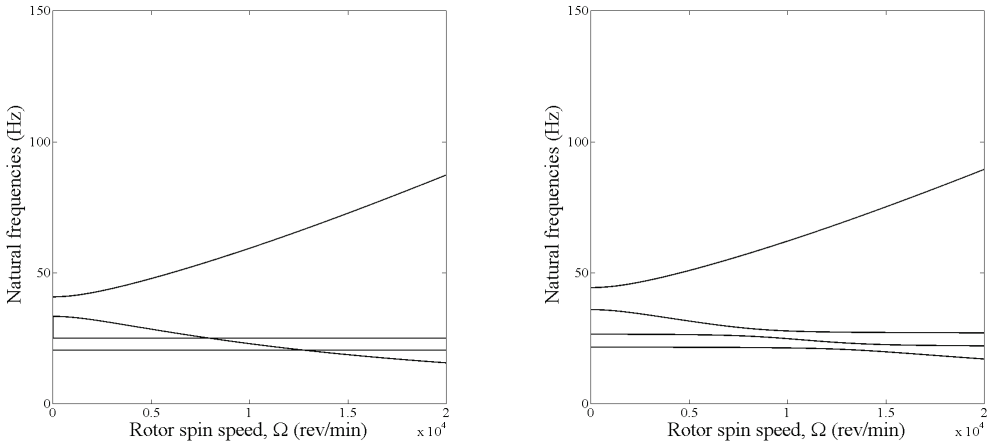

(a) Uncoupled system ($k_{iC} = 0$)

(b) Coupled system ($k_{iC} \neq 0$)

Figure 3: Natural frequency map for a rigid rotor mounted on flexible undamped supports. Cases (a) and (b) refer to a system with symmetric supports or different supports at the two ends respectively.

Figure 4 illustrates the mode shapes for a rigid rotor when the two support bearings are coupled anisotropic bearings, having the same parameters as in the example used for Figure 3b, at four different rotor speeds. The rotor displacement at both bearing locations are depicted. Solid lines connecting the two bearings are established by extending a straight line between each bearing at the same instant. For the first two modes, conical whirl can be observed for all of the rotor speeds except for the first mode at 10000 rev/min. The direction of the rotation is deduced by referring to Figure 4, where counterclockwise motion or forward whirl is positive rotation about the Z axis. However, cylindrical whirls occurred at all speeds, which are backward and forward whirl, for the third and fourth mode respectively except for third mode at 10000 rev/min.

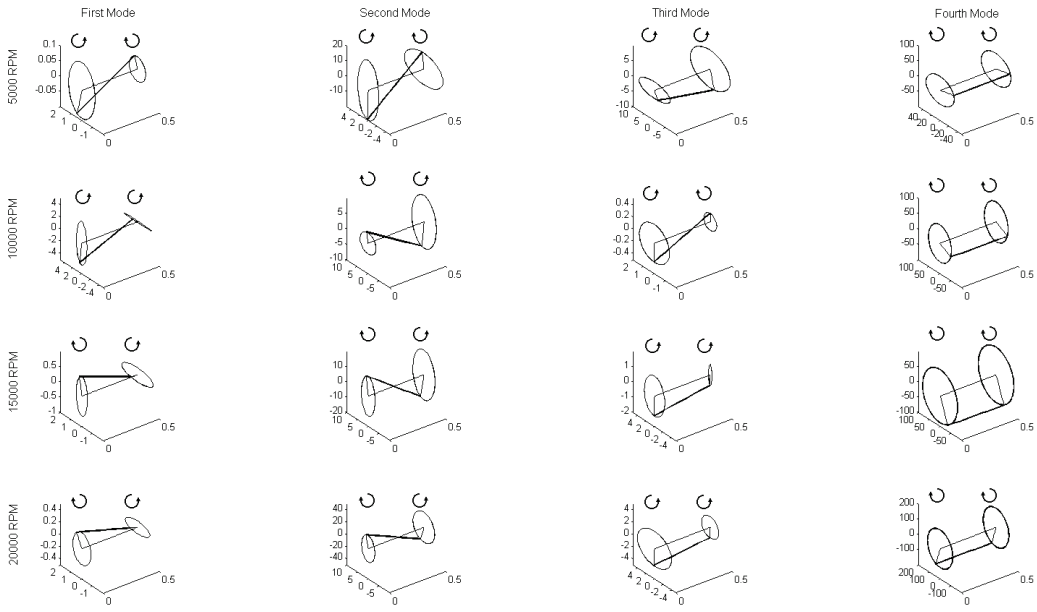

Figure 4: Mode shapes for a rigid rotor mounted on different undamped supports at the ends.

For cases of viscously damped supports, Figure 5 shows comparison of two types of systems namely uncoupled and coupled systems. It can be seen that from case (a) of Figure 5a, two identical natural frequency lines result from solutions of the first and second equations of Eq. (1) because of identical support stiffnesses in the x and y directions. A coupled system is observed in Figure 5b when all the coupling stiffness terms are not the same. Thus the natural frequency lines do not intersect but mode veering [15] is observed for the second and third natural frequency lines.

For the next example, identical viscoelastic supports are consider at both ends of the shaft where the properties of the material are assumed to be identical the x and y directions. Thus is similar to case (a) for viscously damped supports, which have identical stiffnesses in both horizontal and vertical directions at both support ends. Figures 6a and 6b show three different natural frequency lines. From Eq. (10), the first two equations are uncoupled due to the position of the rotor being at the middle of the shaft. Thus the natural frequencies derived from these two equations are identical and independent of Ω. Specifically for case (a) as shown in Figure 6a, the lines of constant natural frequency intersect with a decreasing natural frequency line at about 16000 rev/min. Therefore the first and second equations of Eq. (10) are uncoupled from the third and fourth. For case (b) as in Figure 6b, two distinct natural frequency lines converge as the rotor speed increases due to the gyroscopic terms in the third and fourth equations of Eq. (10).

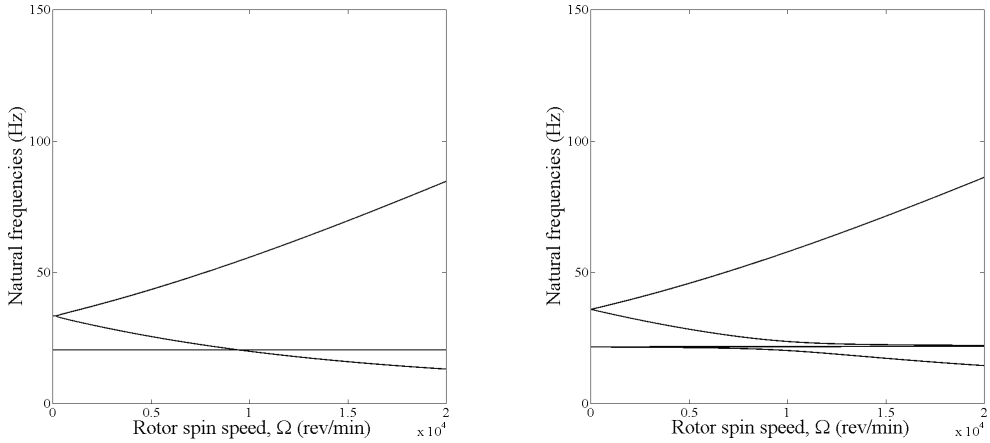

(a) Uncoupled system ($S_{iC} = 0$) (b) Coupled system ($S_{iC} \neq 0$)

Figure 5: Natural frequency map for a rigid rotor mounted on isotropic viscously damped supports.

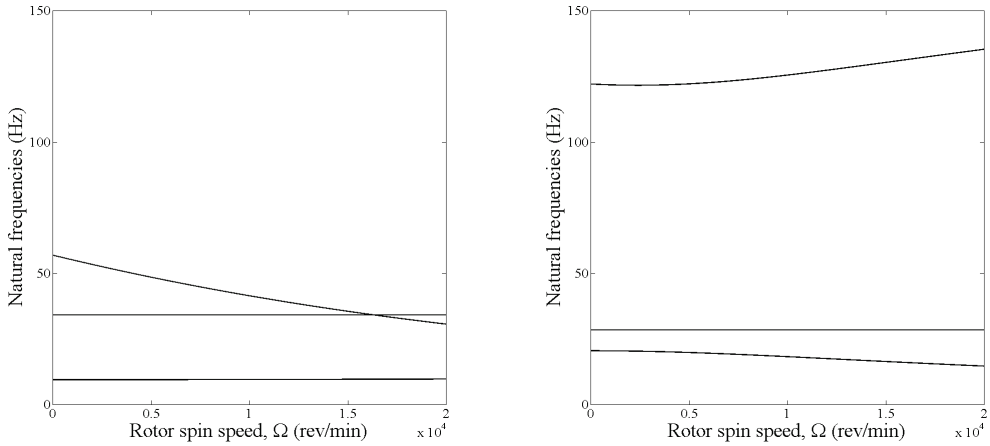

(a) Uncoupled system (b) Coupled system

Figure 6: Natural frequency map for a rigid rotor mounted on identical isotropic viscoelastic supports.

3.2 Forced vibration

In this section, forced vibration analysis is demonstrated specifically for a rotor-bearing system mounted on identical viscoelastic supports, modelled by the standard linear type viscoelastic support with one internal variable. The equations of motion given in Eqs. (11) and (12) are directly integrated using the Runge-Kutta method (available in MATLAB). The steady-state rotor response is obtained at specific rotor speed Ω after considering several thousands cycles of t and plotted throughout certain range of Ω. The response is defined by the x and y displacements of the rotor center and its magnitude is observed from the numerical analysis. Figures 7 and 8 show the displacement magnitude responses of the rotor center and the corresponding loss factor for three different samples of viscoelastic supports respectively. The associated dashed lines with similar colour legend indicates the frequency at which the loss factors are maximum. For both samples A and B, the maximum magnitude of rotor center response are at much lower frequency than corresponding dashed line where frequencies loss factor are 77912 rev/min and 7791 rev/min for sample A and B respectively. Reduction of maximum magnitude response is observed as τ is increased, but the most significant reduction can be seen for sample C where its maximum magnitude response located above its corresponding frequency of maximum loss factor, 779 rev/min. Thus it is suggested that high damping behaviour and higher response attenuation are observed at transition region of the viscoelastic material.

Figure 9 depicts surface plots of the maximum magnitude of the rotor centre and its corresponding resonance frequency. Each of the value is plotted against the pair of $\tau\alpha k_\infty$ and αk_∞ values which corresponds to the damping and stiffness coefficients in Figure 2 respectively. Stiffness value of k_∞ is fix as in Table 1 and variation of α is from 1 to 10 and τ is from $8.6667\text{x}10^{-4}$ to $8.6667\text{x}10^{-3}$. It can be seen that from Figure 9a, in general, the maximum rotor center magnitude responses are decreasing when $\tau\alpha k_\infty$ increases for a specific value of αk_∞. However different observations are found as the stiffness component of αk_∞ is increased for each value of $\tau\alpha k_\infty$. This suggests the prominent effect of the damping element in the viscoelastic material for reducing vibration level of rotor motion. The corresponding resonance frequency at which maximum rotor response occurred is shown by Figure 9b. In general, again, increased values of $\tau\alpha k_\infty$ have a greater effect of shifting the resonance frequency to higher values compared to αk_∞, where the effect can only be seen at medium to high range of $\tau\alpha k_\infty$. This is due to the fact that the stiffness and damper are in parallel in the viscoelastic model introduced.

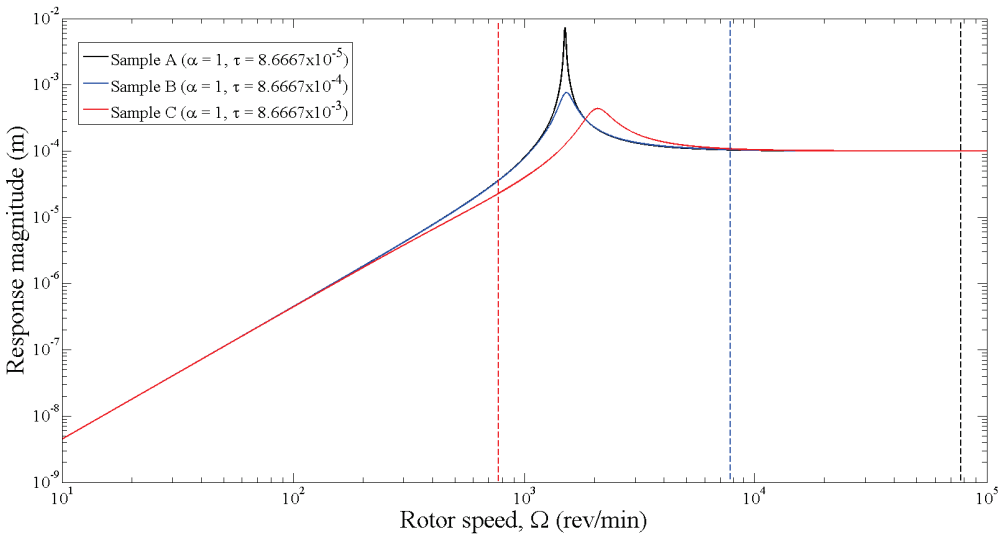

Figure 7: Magnitude of the rotor center displacement response of a rigid rotor mounted on three different samples of identical viscoelastic supports at both shaft's ends (stiff = Sample A, stiffer = Sample B, stiffest = Sample C).

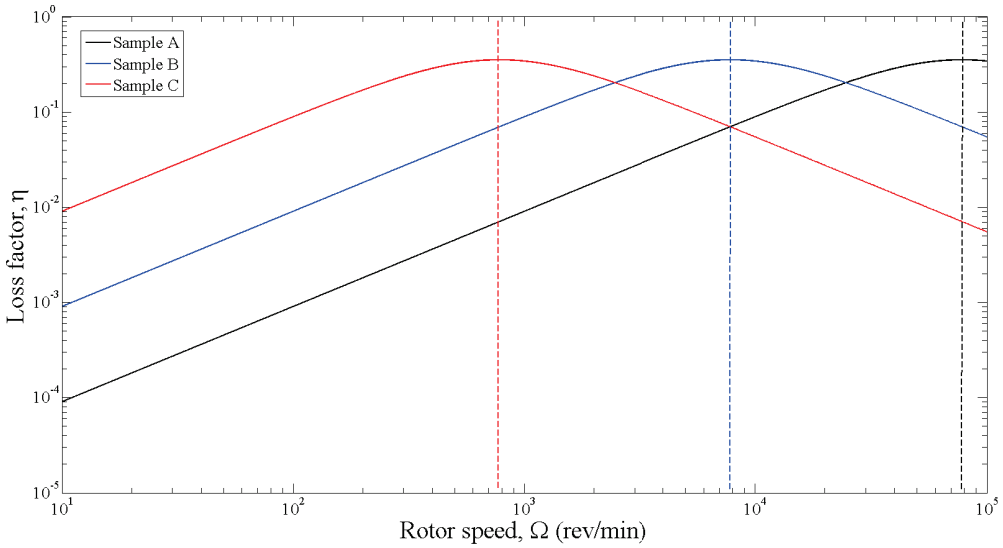

Figure 8: Loss factor of a rigid rotor mounted on three different samples of identical viscoelastic supports (stiff = Sample A, stiffer = Sample B, stiffest = Sample C).

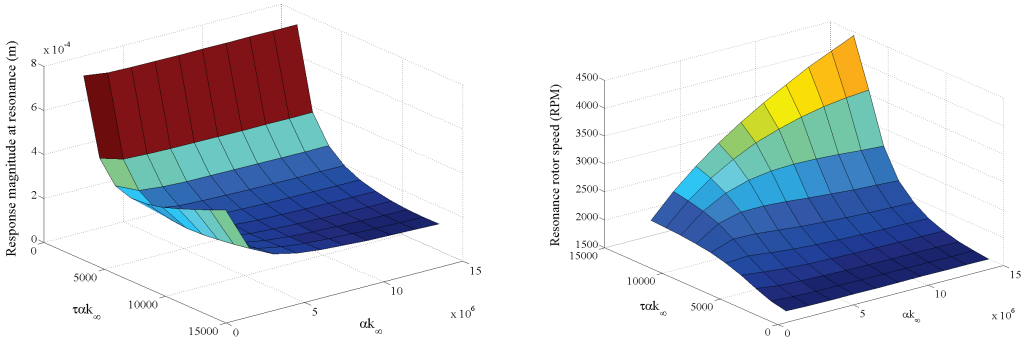

(a) Resonant response magnitude.

(b) Rotor speed for the resonant response.

Figure 9: Resonance speed and maximum displacement response magnitude for a rigid rotor mounted viscoelastic supports.

4 Conclusions

In conclusion, the effect of the stiffness coefficients are dominant in determining the dynamics of the rotor for both elastic and viscoelastic supports. Specifically in terms of mode coupling, the stiffness is significant especially when the supports are not identical at both ends. Furthermore the influence of damping is prominent for attenuating the vibration response explicitly at transition region of viscoelastic material.

REFERENCES

[1] M. Stiassnie, On the application of fractional calculus for the formulation of viscoelastic models. *Applied Mathematical Modelling*, 3(**4**), 300–302, 1979.

[2] A. D. Nashif and J. P. Henderson, *Vibration damping*. John Wiley & Sons, 1985.

[3] R. Fosdick and Y. Ketema, A thermoviscoelastic dynamic vibration absorber. *Journal of Applied Mechanics*, 65(**1**), 17–24, 1998.

[4] M. M. Sjöberg and L. Kari, Non-linear behavior of a rubber isolator system using fractional derivatives. *Vehicle System Dynamics*, 37(**3**), 217–236, 2002.

[5] K. Adolfsson, M. Enelund and P. Olsson, On the fractional order model of viscoelasticity. *Mechanics of Time-Dependent Materials*, 9(**1**), 15–34, 2005.

[6] L. A. Silva, E. M. Austin and D. J. Inman, Time-varying controller for temperature dependent viscoelasticity. *Journal of Vibration and Acoustics*, 127(**3**), 215–222, 2005.

[7] N. Gil-Negrete, J. Vinolas and L. Kari, A nonlinear rubber material model combining fractional order viscoelasticity and amplitude dependent effects. *Journal of Applied Mechanics*, 76(**1**), 011009, 2009.

[8] J. Dutt and B. Nakra, Stability characteristics of rotating systems with journal bearings on viscoelastic support. *Mechanism and Machine Theory*, 31(**6**), 771–779, 1996.

[9] N. Shabaneh and J. W. Zu, Dynamic analysis of rotor–shaft systems with viscoelastically supported bearings. *Mechanism and Machine Theory*, 35(**9**), 1313–1330, 2000.

[10] M. I. Friswell, J. T. Sawicki, D. Inman and A. Lees, The response of rotating machines on viscoelastic supports. *International Review of Mechanical Engineering*, 1(**1**), 32–40, 2007.

[11] H. G. Tillema, Noise reduction of rotating machinery by viscoelastic bearing supports (PhD thesis). *University of Twente*, 2003.

[12] C. A. Bavastri, E. M. d. S. Ferreira, J. J. d. Espíndola and E. M. d. O. Lopes, Modeling of dynamic rotors with flexible bearings due to the use of viscoelastic materials. *Journal of the Brazilian Society of Mechanical Sciences and Engineering*, 30(**1**), 22–29, 2008.

[13] M. I. Friswell, *Dynamics of rotating machines*. Cambridge University Press, 2010.

[14] L. A. Silva, Internal Variable and Temperature Modeling Behavior of Viscoelastic Structures–A Control Analysis (PhD thesis). *Virginia Polytechnic Institute and State University*, 2003.

[15] B. R. Mace and E. Manconi, Wave motion and dispersion phenomena: Veering, locking and strong coupling effects. *The Journal of the Acoustical Society of America*, 131(**2**), 1015–1028, 2012.